

# Spatioangular Prefiltering for Multiview 3D Displays

Vikas Ramachandra, Keigo Hirakawa, *Member, IEEE*,  
Matthias Zwicker, *Member, IEEE*, and Truong Nguyen, *Fellow, IEEE*

**Abstract**—In this paper, we analyze the reproduction of light fields on multiview 3D displays. A three-way interaction between the input light field signal (which is often aliased), the joint spatioangular sampling grids of multiview 3D displays, and the interview light leakage in modern multiview 3D displays is characterized in the joint spatioangular frequency domain. Reconstruction of light fields by all physical 3D displays is prone to light leakage, which means that the reconstruction low-pass filter implemented by the display is too broad in the angular domain. As a result, 3D displays excessively attenuate angular frequencies. Our analysis shows that this reduces sharpness of the images shown in the 3D displays. In this paper, stereoscopic image recovery is recast as a problem of joint spatioangular signal reconstruction. The combination of the 3D display point spread function and human visual system provides the narrow-band low-pass filter which removes spectral replicas in the reconstructed light field on the multiview display. The nonideality of this filter is corrected with the proposed prefiltering. The proposed light field reconstruction method performs light field antialiasing as well as angular sharpening to compensate for the nonideal response of the 3D display. The union of cosets approach which has been used earlier by others is employed here to model the nonrectangular spatioangular sampling grids on a multiview display in a generic fashion. We confirm the effectiveness of our approach in simulation and in physical hardware, and demonstrate improvement over existing techniques.

**Index Terms**—Light field, 3D, autostereoscopic display, lenticular, parallax barrier, sampling, aliasing, crosstalk, sharpening.

## 1 INTRODUCTION

FOR many years, the display of three-dimensional images inspired the imagination and ingenuity of engineers and inventors. One such technology, *multiview 3D display*, admits realization of stereoscopic 3D images from any viewpoint without special glasses. They hold great promise for the future of television and digital entertainment.

In a modern multiview 3D display, a continuous light field is recovered from a set of 2D camera images that form angular samples (views). The 3D display uses spatial multiplexing of these different angular components (views) on the LCD screen matrix, in combination with parallax barriers or lenticular prints [3]. The parallax barrier or lenticular sheet is placed at a small distance in front of the LCD screen. Together, the combination of the LCD screen and the barrier or lenticular sheet reconstructs a continuous light field. It has been shown that a slanted barrier or lenticular helps reduce the so-called “picket fence” or “flipping views” effect resulting from the black barrier mask around each pixel, and is now a part of the standard design for commercial 3D multiview displays (see van

Berkel and Clarke [3], for details). Reduction of the “picket fence” effect is deemed very important for a natural 3D viewing experience. Another advantage of using slanted barriers and lenticulars in conjunction with the LCD screen is that this setup enables easier angular interpolation between adjacent samples (views), giving a smooth visual effect for the reconstructed light field. Yet another reason for the use of slanted lenticular/barriers is that this makes it possible to balance the loss of vertical and horizontal spatial resolution. In the case of vertical lenticulars/barriers, all loss of spatial resolution is horizontal, and there is no loss in the vertical direction.

However, one main drawback of the slanted barrier or lenticular arrangements is that they are prone to light leakage that results in a reduction of image sharpness during light field reconstruction on the 3D display. This is due to the low-pass properties of the display’s angular point spread function (PSF) resulting from the physical design. Henceforth, we use the terms light leakage and angular PSF interchangeably.

The three-way interaction between the input light field signal, the joint spatioangular sampling grid, and the interview light leakage on the physical display complicate stereoscopic image reconstruction. Unlike an ordinary 2D display, artifacts in 3D displays are often severe, examples of which including interview blur and double edges. Existing studies of light leakage [1] and light field aliasing due to joint spatioangular sampling [2], [6], [7], [8] have treated these problems as disjoint and, therefore, provide an incomplete description. The light leakage between views has been referred to previously as monocular crosstalk [1], [4]—a term which we avoid in this paper to prevent confusion with binocular crosstalk present in conventional stereoscopic (two-view) displays. The angular domain has also been called viewspace or intersperspective domain [8].

- V. Ramachandra is with Qualcomm Inc., AV 635F, 5775 Morehouse Drive, San Diego, CA 92121. E-mail: vikas.ramachandra@gmail.com.
- K. Hirakawa is with the Electrical and Computer Engineering Department, University of Dayton, Kettering Laboratories, room 241C, 300 College Park, Dayton, OH 45469. E-mail: k.hirakawa@notes.udayton.edu.
- M. Zwicker and T. Nguyen are with the Computer Science and Engineering Department, UC San Diego, 9500 Gilman Drive, La Jolla, CA 92093. E-mail: zwicker@iam.umibe.ch, nguyent@ece.ucsd.edu.

Manuscript received 13 Sept. 2009; revised 17 Jan. 2010; accepted 8 Feb. 2010; published online 2 June 2010.

Recommended for acceptance by A. Steed.

For information on obtaining reprints of this article, please send e-mail to: [tcvg@computer.org](mailto:tcvg@computer.org), and reference IEEECS Log Number TVCG-2009-09-0217. Digital Object Identifier no. 10.1109/TVCG.2010.86.

The focus of this paper is a rigorous treatment of light field reconstruction on multiview 3D displays. We pose the continuous light field recovery formally as a “reconstruction” of the joint spatioangular signal based on a decomposition of the subsampled or discretized light field signal (in the form of a set of discrete input views) as the principal spectrum and its replicas. Under this formulation, the narrow-band low-pass filtering is carried out by a combination of the human visual system and the physical display hardware. Our aim is to show that the light leakage problem stems from the nonidealities of the reconstruction implementation—we do so by analyzing the influence of the joint spatioangular PSF on joint spatioangular aliasing and inter-view light leakage. To deal with nonrectangular sampling grids on the multiview displays, we use a union of cosets approach as proposed by Jain and Konrad earlier [4]. As detailed in this paper, precise characterization of leakage contamination leads to a well-defined corrective mechanism for minimizing the severity of artifacts. The prefiltering, we propose to correct this effect, is similar in spirit to a temporal sharpening filtering that reduces the ghosting effects on LCD displays with slow black-white response.

Besides the theoretical contributions, we experimentally measure the joint spatioangular PSF of commercially available multiview 3D displays based on a slanted parallax barrier as well as lenticular prints [3]. As mentioned above, these designs have a number of desirable properties. As is consistent with these and other types of multiview 3D display designs, however, our measurements show significant inter-view light leakage. Based on the experimentally measured light leakage, we discuss the development of display-dependent filters and also demonstrate improved image quality on displays based on parallax barriers and lenticular sheets.

The remainder of this paper is organized as follows: Section 1.1 summarizes light field aliasing and its effect on different regions in the 3D scene. This is followed by the analysis of light field signal, sampling, and the light leakage due to the display angular PSF in Section 2 and the development of a prefilter to correct for aliasing and angular blurring in Section 3. Experimental results in simulation and physical display hardware are detailed in Section 4 before making concluding remarks in Section 5.

## 1.1 Previous Work

To date, analysis of light field sampling and reconstruction has drawn from joint spatioangular modeling in the frequency domain [2] and union of cosets for analyzing nonrectangular spatioangular sampling grids [11]. These modeling paradigms give rise to antialiasing schemes using signal processing techniques [8], discretized holographic stereograms [6], the Fourier optics model [7], and lattice theories [11]. Though these antialiasing filters prove effective for idealized multiview 3D displays, the nontrivial interaction of signal reconstruction from samples and nonidealities, such as light leakage due to the angular PSF of the physical displays, have not been made clear.

Previous studies of light leakage have reported (somewhat incorrectly) that it is responsible for spatial blurring as well as double-edge artifacts. To correct these problems, existing solutions have applied spatial processing to control

each view [4], [1]. Owing to the fact that joint spatioangular aliasing [5] and inter-view/angular correlation are ignored, however, these approaches are inadequate for reducing double-edge artifacts and counterbalancing angular blur. Our analysis in Section 2 will make this notion precise.

Our analysis shows that light leakage between views leads to spatioangular blurring which actually has the effect of lessening the aliasing artifacts such as double edges, which arise when a light field is reconstructed from a set of undersampled views. Although this phenomenon was reported previously, the analysis we provide below is contrary to the prior work in this area. Specifically, the work of Jain and Konrad [4] describes a lenticular subsampling process using a modulated train with the gain trailing off from the intended angular positions. However, their model is better characterized as a study of spatial subsampling of each view on the 3D display rather than “crosstalk” albeit its correctness in explaining non-Dirac properties of lenticular prints. As the term “crosstalk” implies, the correct representation should take into account light leakage and aliasing artifacts in the joint spatioangular domain. Leakage involves summation/convolution because the interference between views occurs when light from neighboring views are combined. This cannot be addressed completely by treating light leakage due to the display’s angular PSF as a spatial effect only and processing each view independently as in done by Jain and Konrad. For a complete analysis of the issues involved, light leakage must be analyzed in the joint spatioangular domain. We revisit this point in Section 2.3.

## 2 ANALYSIS OF MULTIVIEW 3D DISPLAYS

Below, the interactions between the input light field signal, sampling, and light leakage due to the display PSF are analyzed. We do so by the way of joint spatioangular modeling [2], [5] (used earlier to model light fields) and the union of cosets approach [12], [11] (used earlier to model nonrectangular sampling grids). The connection between these two modeling paradigms will be made precise in Section 2.3.

### 2.1 Sampling and Aliasing

The relation between the depth and frequency content of a stereoscopic image in the joint spatial-angular domain, and the sampling and reconstruction of light fields is analyzed by Chai et al. [2]. This representation was adopted by Zwicker et al. [5] to analyze the sampled light field in multiview 3D displays [9], which we briefly review below.

Suppose the 3D display reproduces only horizontal parallax (see Fig. 1). In this case, the light rays emitted from a single scan line of a horizontal parallax are parameterized using  $t$ , the angular coordinate as specified by the parallax barrier or lenticular plane index, and  $v$  the (horizontal) spatial coordinate of the high-resolution screen. Let  $x : \mathbb{R}^2 \rightarrow \mathbb{R}$  be a continuous light field. Define  $\Omega_t$  and  $\Omega_v$  to be the angular and spatial frequencies in the separable Fourier transform representation:

$$\hat{x}(\Omega_v, \Omega_t) := \int \int x(v, t) e^{jv\Omega_v + jt\Omega_t} dv dt. \quad (1)$$

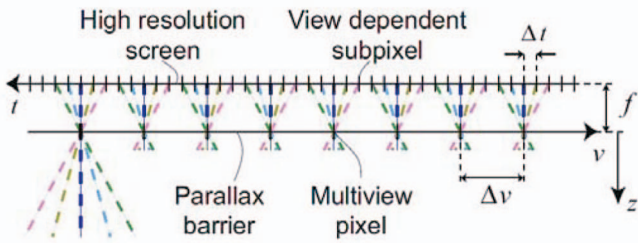


Fig. 1. Parameterization of a scan line of a multiview display and corresponding 2D sampling grid (see [8]).

Owing to the fact that the angular component of a stereoscopic image is uniquely determined by the depth of the object under consideration, the Fourier transform of the light field  $x(v, t)$  is highly structured. In fact, one can show that the light field with a finite depth of field  $(-z, z)$  is “band-limited” in the sense that  $\hat{x}(\Omega_v, \Omega_t) = 0$  when  $z < |\Omega_t/\Omega_v|$ —this notion is illustrated by the spectral support indicated by red in Fig. 2a [2], [5]. Furthermore, the highest concentration of energy is generally found in the low angular and spatial frequency region.

Denote by  $\Delta t$  and  $\Delta v$  the angular and periodic spatial sampling intervals, respectively. By the Poisson summation formula, the spectrum of the discretized light field signal  $x_d$  is a sum of modulated signals:

$$\hat{x}_d(\Omega_v, \Omega_t) = \frac{1}{\Delta v \Delta t} \sum_{\lambda_v \in \frac{2\pi}{\Delta v} \mathbb{Z}} \sum_{\lambda_t \in \frac{2\pi}{\Delta t} \mathbb{Z}} \hat{x}(\Omega_v - \lambda_v, \Omega_t - \lambda_t).$$

Green lines in Fig. 2b mark the spectral support of the replicas, and aliasing occurs when  $\hat{x}(\Omega_v, \Omega_t)$  and  $\hat{x}(\Omega_v - \lambda_v, \Omega_t - \lambda_t)$  have overlapping support. It is clear from the diagram that the aliased components (shaded region) are simultaneously high pass in the spatial and angular axes. In practice, the depth of field  $(-z, z)$  determines the joint spatioangular bandwidth and so the risk of aliasing is light field-dependent. As implied in Fig. 2, the resolution of angular sampling in a typical multiview display is far coarser than the spatial sampling.

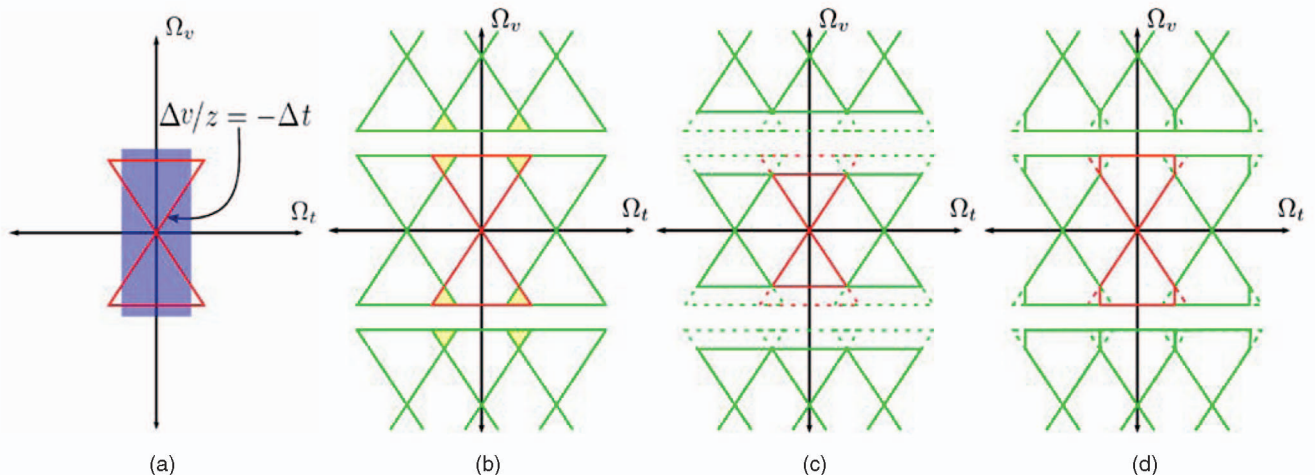


Fig. 2. Spectral support of the light field signal. Red and green lines represent the support of principal and replicated spectra, respectively. Aliased regions are shaded yellow; display bandwidth is shaded blue. (c) and (d) illustrate antialiasing strategies based on spatial and angular processing, respectively. (a) Original signal. (b) Aliased. (c) Spatial antialiasing. (d) Angular antialiasing.

Aliasing due to undersampling of the angular component causes manifestation of double image artifacts, as the examples in Figs. 9a and 10a show. Suppose for a moment that the multiview display is free of light leakage. Then, the joint spatioangular modeling suggests two general categories for antialiasing strategies. The spatial processing paradigm achieves antialiasing by attenuating high spatial frequency components from each view [11], [4]—illustrated in Fig. 2c. Avoiding aliasing requires an aggressive antialiasing approach, however, because it also eliminates frequency components that are not affected by aliasing (high pass in spatial axis and low pass in angular axis). By contrast, the prefiltering of the angular component (illustrated in Fig. 2d) takes better advantage of structure inherent in the light field signal, as only the components that are simultaneously high pass in spatial and angular axes are filtered out [5]. In practice, antialiasing in the spatial paradigm (Fig. 2c) is easier to implement as this involves blurring each view separately. Antialiasing in the angular domain (Fig. 2d) requires the processing of all the input views jointly and simultaneously.

The *display bandwidth* in the joint spatioangular domain (blue box in Fig. 2a) is determined by the Nyquist limit in the usual sense:

$$\hat{h}(\Omega_v, \Omega_t) := \begin{cases} 1, & \text{if } |\Omega_v| \leq \pi/\Delta v, |\Omega_t| \leq \pi/\Delta t, \\ 0, & \text{otherwise.} \end{cases} \quad (2)$$

This also sheds light on the displayable joint spatioangular resolution of the light field. From Fig. 2a, it is clear that the spectral support of the light field at depth  $|z| > \Delta v/\Delta t$  exceeds the angular bandwidth of the display ( $|\Omega_t| = \pi/\Delta t$ ). Hence, the maximal displayable spatial frequency is depth-dependent ( $\Omega_v = \pi/z\Delta v$ ), and as such, region of the light field at larger depths will appear blurry.

## 2.2 Interaction of Aliased Light Field and Light Leakage

The emphasis so far has been on *discretization* of continuous light fields. The overall goal of stereoscopic image reconstruction, however, is to recover a *continuous* light

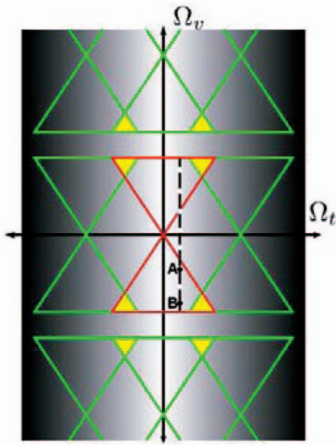


Fig. 3. Angular PSF superimposed on an aliased spectrum of Fig. 2b.

field  $x$  from a set of samples. This is realizable as reconstruction—the process of separating the principal spectrum from its replicas by the way of narrow-band low-pass filtering. Although spatial smoothing is typically handled through blurring inherent in the human visual system, angular low-pass filtering must be carried out by the display’s physical hardware in order to reduce the pixelization artifacts during light field reconstruction. In physical 3D displays, the slanted barrier or lenticular design is used to reduce the pixelization artifacts commonly referred to as “picket fence” or “flipping views.” Thus, the angular slant ensures that the barrier is not visible when the viewer’s eye moves from one view to another. From a signal processing point of view, the slanted barrier is an implementation of an angular low-pass reconstruction filter, which removes spectral replicas in the angular domain. In other words, the resultant interview pixel averaging due to the slanted barriers carries out the angular blurring kernel required for the reconstruction of a sufficiently smooth light field. Such a slanted barrier or lenticular construction also allows for more light to pass through ensuring better brightness for 3D displays. However, the above-mentioned setup also results in light from one view leaking into adjacent views. Thus, the 3D angular reconstruction blur kernel leads to interview light leakage.

Due to this, the human observer of multiview display sees a linear combination of neighboring views. Although this helps achieve a smoother light field perception, one of its unintended consequences is the interview contamination.

In this section, we analyze the trade-offs between stereoscopic image reconstruction and light leakage. When the smoothing is (angular) translation invariant, this phenomenon is modeled precisely by an angular point spread function  $f(t)$  acting on the subsampled light field  $x_d$  regardless of the spatial context of the signal. By the separability of the Fourier transform and the convolution theorem, the overall effect is

$$\{\hat{f} \cdot \hat{x}_d\} = \frac{1}{\Delta v \Delta t} \sum_{\lambda_v \in \frac{2\pi}{\Delta v} \mathbf{Z}} \sum_{\lambda_t \in \frac{2\pi}{\Delta t} \mathbf{Z}} \hat{f}(\Omega_t) \hat{x}(\Omega_v - \lambda_v, \Omega_t - \lambda_t). \quad (3)$$

Fig. 3 shows the gray-scale coded frequency response of a typical light leakage kernel  $f$ , which is inherently low pass, i.e., darker shades indicate greater attenuation. The spectral

replica due to the modulated light field  $\hat{x}(\Omega_v - \lambda_v, \Omega_t - \lambda_t)$  is attenuated heavily, thanks to the modulation by high frequencies  $\lambda_t$  and the rapid decay of the low-pass frequency response  $\hat{f}(\Omega_t)$ . Indeed, the double-edge aliasing artifacts are softened, as Figs. 9b and 10b show. The baseband signal  $\hat{x}(\Omega_v, \Omega_t)$  is “smoothed” by the angular PSF  $\hat{f}(\Omega_t)$ , however—the effect of which is an interview blurring that results in diminished depth discrimination and a spatial blurring effect. As a result of this spatial blurring effect, the light field reconstructed on the display looks washed out and loses sharper spatial details such as sharp spatial edges and fine texture information.

A closer look into (3) reveals that high angular frequency components are attenuated by the angular frequency response regardless of their spatial content, i.e., regions of high and low spatial frequency components are affected equally. This is illustrated by points A and B in Fig. 3; both points have the same angular frequency and are subject to the same amount of angular blur, although point B lies in a higher spatial frequency region compared to point A. Furthermore, although double-edge artifacts appear less pronounced, aliasing is not completely “undone” by light leakage due to the angular PSF. To see this, consider the case where the baseband  $\hat{x}(\Omega_v, \Omega_t)$  intersects a nontrivial modulated signal  $\hat{x}(\Omega_v - \lambda_v, \Omega_t - \lambda_t)$ . The aliasing in the presence of light leakage is commensurate with aliasing in a leakage-free multiview display because the angular PSF attenuates the baseband and the aliased component by an equal amount—that is, the ratio of  $\hat{f}(\Omega_t) \hat{x}(\Omega_v, \Omega_t)$  to  $\hat{f}(\Omega_t) \hat{x}(\Omega_v - \lambda_v, \Omega_t - \lambda_t)$  is the same as  $\hat{x}(\Omega_v, \Omega_t)$  to  $\hat{x}(\Omega_v - \lambda_v, \Omega_t - \lambda_t)$ . Therefore, proper stereoscopic image reconstruction requires a combination of antialiasing and angular sharpening. Angular sharpening means suitable prefiltering of the light field signal to compensate for the low-pass characteristic of the angular PSF of the 3D display.

### 2.3 Generalized Joint Spatioangular Analysis Using Union of Cosets

The two-dimensional analysis (1D spatial and 1D angular) studied thus far can be generalized to a full stereoscopic image reconstruction on a two-dimensional surface by extending it to three dimensions (2D spatial and 1D angular; only the horizontal angular component is considered) [2]. The goal of this section is to incorporate the joint spatioangular model into the *union of cosets* representation of nonrectangular sampling grids presented by Konrad and Agniel [11]—which has been used previously to characterize 2D spatial sampling in multiview displays, and analyze the interaction between aliasing and light leakage therein. We do so by exploiting interview correlation as suggested by the joint spatioangular model from the previous section.

We start with a brief introduction to the union of cosets approach to model lattices or sampling grids. A uniform lattice  $\Lambda \subset \mathbb{R}^n$  comprises a discrete subgroup of an  $n$ -dimensional euclidean space. We say a nonsingular matrix  $N$  having real entries generates a point lattice  $\Lambda_N$  if  $\Lambda_N = N\mathbb{Z}^n$ , in which case columns of  $N \in \mathbb{Z}^{2 \times 2}$  are said to form a basis for the lattice.  $N$  is often called the sampling matrix as it generates a periodic (sampling) pattern indexed by  $n$ -tuples of integers which corresponds to the lattice  $\Lambda_N$ .

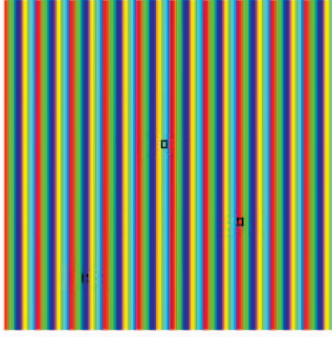


Fig. 4. A simple union of cosets sampling grid example. Each color represents the sampling grid for a given view. Five views are multiplexed to form the complete 2D grid. The sampling grids of all views are translates of a single subsampling pattern governed by the sampling matrix  $N$ . Black boxes are used to indicate some example pixels.

The set of distinct translates of  $\Lambda_N$  by vectors  $\{\psi_m\}_{m \in \{1, \dots, M\}}$  is said to form a set of *cosets* in  $\mathbb{Z}^n$ . The key point is that  $\mathbb{Z}^n$  can be written as a union of cosets, that is  $\bigcup_m \{\Lambda_N - \psi_m\} = \mathbb{Z}^n$ .

In the context of multiview displays, the display spatially combines a set of input views to fill the available (integer indexed) pixel grid on the LCD matrix which can be represented as the uniform lattice  $\mathbb{Z}^2$ , where  $\mathbb{Z}$  is the set of integers. The associated spatial sampling pattern for each view may then be represented by a less dense lattice. We call this spatially multiplexed LCD image the *composite image*.

More precisely, redefine the light field  $x(v, t)$  as a three-dimensional signal (where  $v \in \mathbb{R}^2$  and  $t \in \mathbb{R}$ ). Let  $M$  be the number of input views. For  $m \in \{1, \dots, M\}$ , the composite image  $x_c$  is generated by spatially multiplexing different views and by making correspondences between cosets and angular samples:

$$x_c(Nn - \psi_m) := x(Nn, \Delta t \cdot m),$$

where  $n$  is the spatial index and each coset vector  $\Lambda_N - \psi_m$  corresponds to the spatial sampling grid of the  $m$ th view.

A simple illustration of this concept is provided in Fig. 4. A complete 2D grid shown in the figure consists of five multiplexed view sampling grids. The sampling grid of each view is coded with a particular color. The sampling matrix  $N$ , in this case, is given by  $N = \begin{bmatrix} 5 & 0 \\ 0 & 1 \end{bmatrix}$  which defines  $\Lambda_N + 0$ —the spatial sampling corresponding to the “first view”—and the other views are represented by horizontal translates of  $\Lambda_N$ , that is  $\psi_m \in \{[0, 0]^T, \dots, [4, 0]^T\}$ .

The corresponding Fourier transform (where  $\Omega_v \in \mathbb{R}^2$ ) is

$$\begin{aligned} \hat{x}_c(\Omega_v) &:= \sum_n x_c(n) e^{j\Omega_v^T n} \\ &= \sum_{\lambda_v \in \hat{\Lambda}} \sum_{m \in \mathbb{M}} \frac{e^{j\Omega_v^T \psi_m}}{\det(N)} \int x(v, \Delta t \cdot m) e^{j(\Omega_v - \lambda_v)^T v} dv, \end{aligned}$$

where  $\hat{\Lambda} := \{2\pi N^{-T} \mathbb{Z}^2\}$  is the dual lattice and  $e^{j\Omega_v^T \psi_m}$  is the result of spatial translation by  $\psi_m$ . In order that this makes sense with the construction of a multiview display, assume  $\psi_m = \psi \cdot m$  for some vector  $\psi \in \mathbb{R}^2$ . This means that the sampling grids of different views are translates of each other, which is true for multiview displays. Then, the

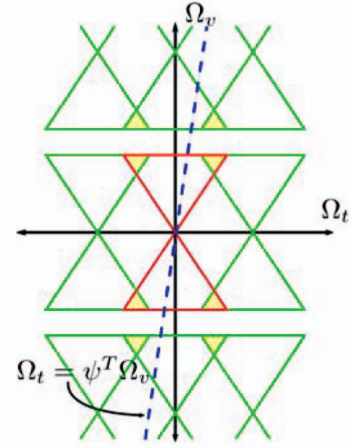


Fig. 5. The trajectory of  $\Omega_t = \psi^T \Omega_v$  over the joint spatioangular Fourier transform  $\hat{x}(\Omega_v, \Omega_t)$  represents the spatial Fourier transform of the composite image,  $\hat{x}_c(\Omega_v)$ . This figure summarizes the relation between the two modeling paradigms (the spatioangular light field model and the union of cosets model).

summation over  $m$  above results in a *discrete time* Fourier transform, and

$$\begin{aligned} \hat{x}_c(\Omega_v) &= \sum_{\lambda_v \in \hat{\Lambda}} \sum_{m \in \mathbb{M}} \frac{e^{j\Omega_v^T (\psi \cdot m)}}{\det(N)} \int x(v, \Delta t \cdot m) e^{j(\Omega_v - \lambda_v)^T v} dv \\ &= \frac{1}{\det(N) \Delta t} \sum_{\lambda_v \in \hat{\Lambda}} \sum_{\lambda_t \in \frac{2\pi}{\Delta t} \mathbb{Z}} \hat{x}(\Omega_v - \lambda_v, \psi^T \Omega_v - \lambda_t), \end{aligned} \quad (4)$$

where  $\hat{x}(\cdot, \cdot)$  is the joint spatioangular Fourier transform in the sense of (1). Owing to the tight coupling of angular and spatial indices in the composite image, the angular component of  $\hat{x}(\cdot, \cdot)$  is now indexed by the spatial frequency. It is clear from the *summation over modulation* by  $(\lambda_v, \lambda_t)$  that the maximal display bandwidth in this generalized joint spatioangular multiplex model is determined by

$$\hat{h}(\Omega_v, \Omega_t) := \begin{cases} 1, & \text{if } \Omega_v \in 2\pi N^{-T} [-\frac{1}{2}, \frac{1}{2}]^2 \text{ and } |\Omega_t| \leq \pi / \Delta t, \\ 0, & \text{otherwise.} \end{cases} \quad (5)$$

The spatial bandwidth (i.e.,  $\Omega_v \in 2\pi N^{-T} [-\frac{1}{2}, \frac{1}{2}]^2$ ) is in agreement with the work of Konrad and Agniel [11]; the angular bandwidth (i.e.,  $|\Omega_t| \leq \pi / \Delta t$ ) is consistent with the work of Zwicker et al. [5]. The model, as described by (4) and (5), however, is a more complete treatment of the generalized joint spatioangular multiplexing in multiview 3D displays. Fig. 5 illustrates the horizontal parallax example, where the information captured by  $\hat{x}_c$  is represented by the trajectory of the line  $\Omega_t = \psi^T \Omega_v$  over the joint spatioangular Fourier domain.

Suppose now we are concerned with light leakage, modeled by  $f(t)$  as before. It follows from (4) that the Fourier transform of the contaminated multiplexed light field signal is

$$\begin{aligned} &\frac{1}{\det(N) \Delta t} \sum_{\lambda_v \in \hat{\Lambda}} \sum_{\lambda_t \in \frac{2\pi}{\Delta t} \mathbb{Z}} \hat{f}(\psi^T \Omega_v) \hat{x}(\Omega_v - \lambda_v, \psi^T \Omega_v - \lambda_t) \\ &= \hat{f}(\psi^T \Omega_v) \cdot \hat{x}_c(\Omega_v). \end{aligned} \quad (6)$$

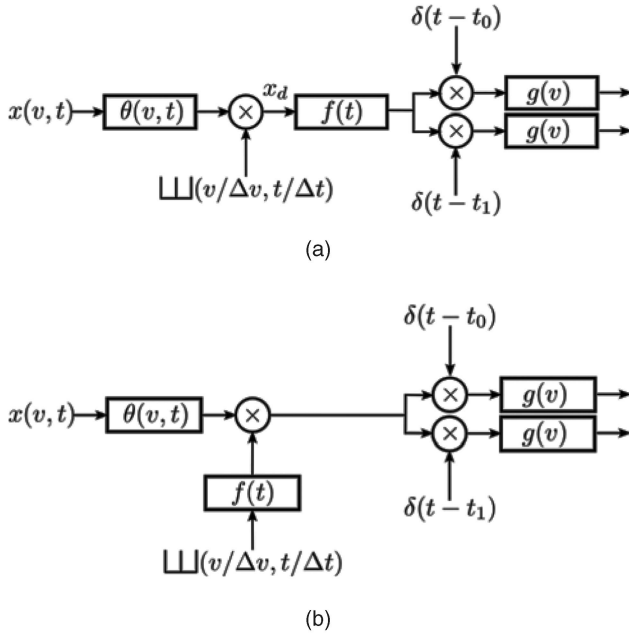


Fig. 6. Models of multiview 3D display, where the output represents what the human observer sees. Here,  $\theta$  is prefiltering (antialiasing, etc.);  $f$  is light leakage; and  $g$  is spatial blur in vision. Discretization of a continuous light field is denoted by sampling. The observer's position determines which views are seen through the parallax barrier (or the lenticular print). Notice that in the proposed scheme,  $f(t)$  models the angular blur between views, unlike the model by Jain and Konrad which models  $f(t)$  as a spatial blur on each view. See Section 2.3. (a) Model with light leakage (Section 2). (b) Model by Jain and Konrad [4].

The key point here is that the light leakage kernel  $f(t)$  can be interpreted as a *spatial operator* over the composite image  $x_c$ , simplifying our analysis significantly (compare (3) and (6)). This also enables us to incorporate the nonrectangular sampling grids for each view—this is not possible without the use of the idea of the composite image. In other words, the composite image discussion helps us treat the angular leakage phenomenon as a spatial operator over the composite image, while at the same time taking into account the nonrectangular spatial sampling of each view on the LCD matrix. When  $\psi = [0, 1]^T$  and  $N = [1, 0; 0, M]$ , (6) agrees with the horizontal parallax model studied in the previous section.

Finally, the analysis in (6) is contrary to the previous work in this area. According to Jain and Konrad [4], the subsampled light field signal subject to  $f$  is

$$\frac{1}{\det(N)\Delta t} \sum_{\lambda_v \in \Lambda} \sum_{\lambda_t \in \frac{2\pi}{\Delta t}\mathbf{Z}} \hat{f}(\psi^T \lambda_v) \hat{x}(\Omega_v - \lambda_v, \psi^T \Omega_v - \lambda_t) \quad (7)$$

$$= \hat{f}(\psi^T \lambda_v) \cdot \hat{x}_c(\Omega_v).$$

(In this setting, the aliasing is weakened relative to the baseband because  $\|\hat{f}(0)\| \geq \|\hat{f}(\psi^T \lambda_v)\|$  when  $\lambda_v \neq 0$ .) This stems from interpreting the *crosstalk or leakage* as a modification to the spatial multiplexing process itself which in turn leads to the interpretation that it is an intraview spatial operator (as indicated by  $\psi^T \lambda_v$ ), rather than modeling the combining of the neighboring views due to the leakage of light (as indicated by  $\hat{f}(\Omega_t)$  for the spatioangular light field or equivalently,  $\hat{f}(\psi^T \Omega_v)$  over the composite image)—see Fig. 6b.

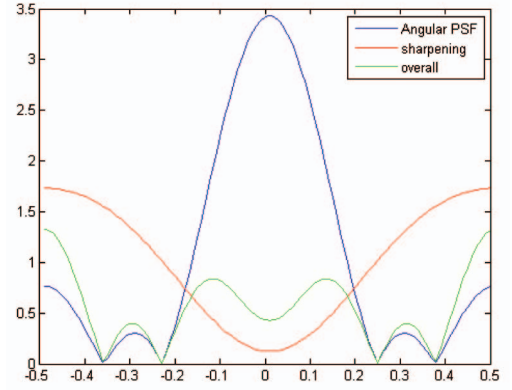


Fig. 7. Angular frequency response of the angular blurring (light leakage) kernel and the corresponding sharpening prefiltering for the Newsight parallax barrier display. The overall response is the product to the two.

As the angular PSF  $f$  in hardware operates on subsampled light field  $x_c$  instead of the complete signal  $x$ , it would be more accurate to include the interference between views rather than modeling the pointwise “unequal gain” of the optics. Thus, the conclusion reached in (7)—that crosstalk increases the effective bandwidth of the display device—is not appropriate, in general, for the light leakage problems under our consideration. It is worth noting that (6) and (7) are equal when  $x(\Omega_v, \Omega_t)$  is supported only on the “zero disparity plane” (i.e.,  $\hat{x}(\Omega_v, \Omega_t) = 0, \forall \Omega_t \neq 0$ )—that is, the light leakage analysis by Jain and Konrad [4] is valid only in this special case. As there is no angular aliasing in this scenario (and the spatial components are unaffected), however, this is now a purely spatial sampling problem—angular leakage has no effect, and spatioangular bandwidth of the display is unaffected. In contrast, the proposed framework presents a complete picture of light leakage as a joint spatioangular effect.

### 3 ANTIALIASING AND ANGULAR SHARPENING STRATEGIES

Recall that the interview smoothing kernel  $f(t)$  gives rise to (angular) reconstruction. Owing to the nonidealities of physical hardware, however, the low-pass filter has neither a flat pass-band (to preserve the principal spectrum) nor a sharp cutoff (to attenuate the modulated spectral replica). Indeed, the interview point spread function of a real hardware that we measured experimentally confirms this—see Figs. 7 and 8. In order to reconstruct the continuous light field  $x$  as faithfully as possible via the 3D multiview display, we propose a prefiltering approach to addressing the twin problem of aliasing and light leakage.

To make this notion precise, define  $g(v)$  to be a combination of the LCD spatial blur kernel and the spatial smoothing kernel inherent in human visual system [13], [14]. We are interested in designing the prefiltering  $\theta(v, t)$  that minimizes the error between the continuous light field  $\{g \star x\}(v, t_0)$  and the reconstructed light field  $\{g \star f \star (\theta \star x)_d\}(v, t_0)$  or  $\{g \star f \star (\theta \star x)_c\}(v, t_0)$ , where  $\cdot_d$  and  $\cdot_c$  denote discretization in terms of the spatioangular light field and the composite image, respectively, as described in the previous section,  $\star$  is the convolution operator, and the observer's position  $t_0 \in \mathbb{R}$  determines which view is seen

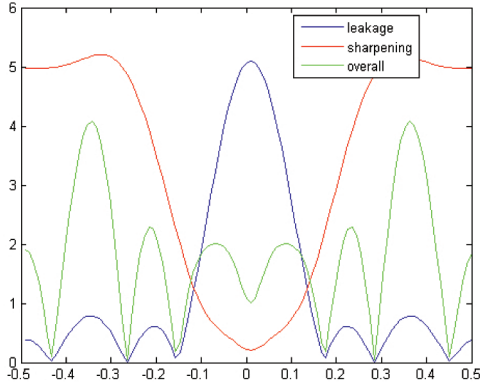


Fig. 8. Angular frequency response of the angular blurring (light leakage) kernel and the corresponding sharpening prefiltering for the Alioscopy lenticular display. The overall response is the product to the two.

through the parallax barrier (or the lenticular print). Under this formulation, the reconstruction error  $E_R$  can be categorized into two parts:

$$\{E_R\} = (\{\hat{g} \cdot \hat{f} \cdot \hat{\theta}\} - \hat{g})\hat{x} + \sum_{\substack{(\lambda_v, \lambda_t) \\ \neq (0,0)}} \hat{g}(\Omega_v)\hat{f}(\Omega_t)\{\hat{x} \cdot \hat{\theta}\}(\Omega_v - \lambda_v, \Omega_t - \lambda_t).$$

Here, the first term measures fidelity since it tries to minimize the error between the true signal which needs to be seen the observer and the signal which is actually seen. The second term is the energy of the nonprincipal spectral replicas, which needs to be minimized during reconstruction. Intuitively, the prefiltering  $\hat{\theta}$  takes on the role of angular and spatial “sharpening” in the fidelity term by flattening  $\hat{g} \cdot \hat{f} \cdot \hat{\theta}$  in the pass-band—this has the effect of restoring the interview discrimination. On the other hand,  $\hat{\theta}$  that minimizes  $\hat{g}(\Omega_v)\hat{f}(\Omega_t)\hat{\theta}(\Omega_v - \lambda_v, \Omega_t - \lambda_t)$  reduces the error stemming from aliasing by filtering out the spectral replicas.

As is by now a standard practice, a nonparametric approach to designing  $\hat{\theta}$  (i.e., assuming no correlation in  $\hat{x}$ ) is to minimize the cost function

$$J := \|\{\hat{g} \cdot \hat{f} \cdot \hat{\theta}\} - \hat{g}\|^2 + \sum_{\substack{(\lambda_v, \lambda_t) \\ \neq (0,0)}} \|\hat{g}(\Omega_v)\hat{f}(\Omega_t)\hat{\theta}(\Omega_v - \lambda_v, \Omega_t - \lambda_t)\|^2.$$

Setting  $\partial J / \partial \hat{\theta}(\Omega_v, \Omega_t)$  to zero and solving for  $\hat{\theta}$ , the  $L^2$  optimal prefiltering takes the form of

$$\hat{\theta}_{\text{opt}}(\Omega_v, \Omega_t) = \frac{|\hat{g}^2(\Omega_v)\hat{f}(\Omega_t)|}{\sum_{\lambda_v, \lambda_t} |\hat{g}(\Omega_v - \lambda_v)\hat{f}(\Omega_t - \lambda_t)|^2}. \quad (8)$$

One notable feature is that when  $\hat{f}$  and  $\hat{g}$  represent ideal low-pass filters, the antialiasing filter defined in (2) is recovered. Moreover, supposing that the spatial sampling is sufficiently dense and  $g(v)$  and  $f(t)$  have sufficiently sharp cutoff, we make the following approximation:

$$\{\hat{g} \cdot \hat{f}\} \approx \hat{f}(\Omega_t)\hat{h}(\Omega_v, \Omega_t),$$

where  $\hat{h}$  is the ideal low-pass filter of (2). What this assumption practically means is that the signal is over-sampled in the spatioangular domain to get rid of any aliasing present. Then, it follows that antialiasing and angular sharpening in  $\hat{\theta}_{\text{opt}}$  are *separable*:

$$\hat{\theta}_{\text{opt}}(\Omega_v, \Omega_t) = \frac{\hat{h}(\Omega_v, \Omega_t)}{|\hat{f}(\Omega_t)|}. \quad (9)$$

This implies that one could first antialias the input light field and then perform a prefiltering step (to counter the display’s angular PSF) before the continuous light field is reconstructed on the display.

## 4 IMPLEMENTATIONAL DETAILS AND EXPERIMENTAL RESULTS

### 4.1 Angular Point Spread Measurement

Following a procedure similar to the one described by Jain and Konrad [4], we measured the angular point spread function of a Newsight 32 inch parallax barrier multiview display and an Alioscopy 22 inch lenticular display. The parallax barrier display hardware resolution supports five views and  $1,366 \times 768$  pixels in full color. The lenticular display hardware resolution supports eight views and  $1,920 \times 1,080$  pixels in full color. The displays were configured to show an “angular impulse function”  $x(v, t) = \delta(t)$  by setting one view to a solid red and all others to black. The light leakage then is directly observable by cameras positioned to see all views from a suitable viewer distance. The measured coefficients of the 1D angular PSF revealed an almost symmetric structure. The 1D angular PSF for the parallax barrier display was measured as

$$f(\Delta t \cdot m) = [0.5488, 0.6664, 1.0000, 0.6664, 0.5488].$$

The 1D angular PSF for the lenticular display was measured as

$$f(\Delta t \cdot m) = [0.59, 0.679, 0.781, 1.0000, 0.781, 0.679, 0.59].$$

The angular frequency response of the parallax barrier blurring kernel and the lenticular kernel are shown in Figs. 7 and 8; our measurements agree qualitatively with what is reported by Jain and Konrad [4]. Note that the smooth curves in the angular frequency domain are obtained with suitable zero padding.

The experimental results of the sequel is implemented with the separable filter approach of (9). The discretized angular sharpening filter (after the antialiasing step) for the parallax barrier and lenticular displays are

$$\tilde{f}(\Delta t \cdot m) = [-0.0361, -0.4020, 1.0000, -0.4020, -0.0361]$$

and

$$\tilde{f}(\Delta t \cdot m) = [0.05, -0.14, -0.38, 1.0, -0.38, -0.14, 0.05],$$

respectively. These are the proposed prefilters used to generate results in the next section for the parallax barrier and lenticular displays. These filters are designed as the pseudoinverse of  $f$  and their angular frequency responses are shown in Figs. 7 and 8. In practice, the prefiltering is implemented as circular convolution to wrap around the

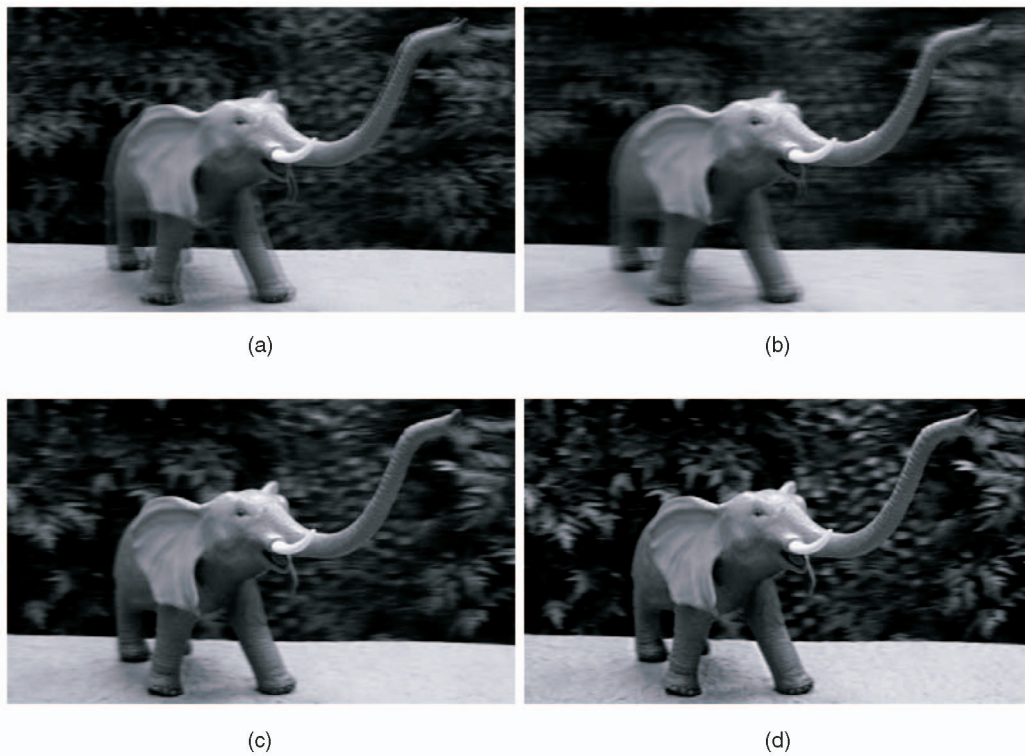


Fig. 9. Simulated multiview display of “Elephant” image. (a) The angular aliasing (double image) artifacts. (b) shows that light leakage decreases double images. (c) The antialiased light field (no double images, blurry due to angular PSF). (d) The proposed scheme (sharper output, angular PSF is precompensated). (a) Corrupted by aliasing (PSNR 24.38 dB). (b) Corrupted by aliasing and light leakage (PSNR 24.72 dB). (c) With antialias filter [5] (PSNR 25.13 dB). (d) With proposed prefilter after antialiasing (PSNR 25.69 dB).

angular samples on the boundaries—this is valid because the “last view” of each viewing zone is followed by the “first view” of the neighboring viewing zone.

The antialiasing component of (9) was implemented according to the model proposed by Zwicker et al. [5]. To summarize antialiasing, the input light field was highly upsampled to remove angular aliasing in the input. The light field was then sheared such that the zero disparity plane lies in the desired image region (face of the elephant for the “Elephant” image, and front of the train for the “Train” image) and cropped. Then, a 1D Gaussian angular low-pass filter was used, with  $\sigma = 0.75$  to avoid overly blurry results on the display.

## 4.2 Results

The effectiveness of the proposed prefiltering approach is verified by reconstructing stereoscopic images in simulation and in physical display hardware. The proposed angular sharpening prefilter which is used in this section is the same as  $f(m)$  discussed in the previous section. The simulation results are shown in Figs. 9 and 10 for the “Elephant” and “Train” light fields. This confirms that aliasing due to joint spatioangular subsampling results in double-edge artifacts (Figs. 9a and 10a), which are subsequently softened by the presence of light leakage as seen in Figs. 9b and 10b (though not eliminated completely). The angular PSF used to generate the simulation results is  $f(\Delta t \cdot m)$  from the previous section. The joint spatioangular antialiasing filter by Zwicker et al. [5] applied prior to sampling prevents the manifestation of double edges successfully (Figs. 9c and 10c).

After antialiasing, a closer examination reveals that some objects in the image, especially those found in the background, appear blurry due to the angular PSF effect. The joint spatioangular antialiasing and proposed angular sharpening of (8) corrects this problem, as evidenced by the sharpened appearance of the background (Figs. 9d and 10d).

Analysis of Section 3 suggests that the blurriness in Figs. 9c and 10c is not a spatial smear, but rather an angular blur caused by the angular point spread function. In fact the blur is strongest in the regions of the light field with the highest angular frequency, as the attenuation by the kernel  $f(t)$  is the heaviest. As a result, the human observer of multiview display experiences a weakened depth perception<sup>1</sup> as it is difficult to resolve the background. As such, it would be misleading to assume that spatial processing will correct this problem. Indeed, the main difference between the proposed prefiltering and the prior art is that we recover both the foreground and the background objects (see Figs. 15 and 16). Note also that all methods adequately reconstruct the zero disparity plane (foreground), where all views are identical and only the DC angular frequency is supported.

The performance of the prefiltering was also tested using a Newsight 32 inch parallax barrier multiview display as well as a 22 inch Alioscopy lenticular display. The screen captures of the reconstructed images using a seven megapixel camera are shown in Figs. 11, 12, 13, and 14. As is consistent with the results of simulation studies, the reconstructed light field signal is free of double edges and is

1. We are unable to illustrate this point in this paper owing to the limitations of printed media.

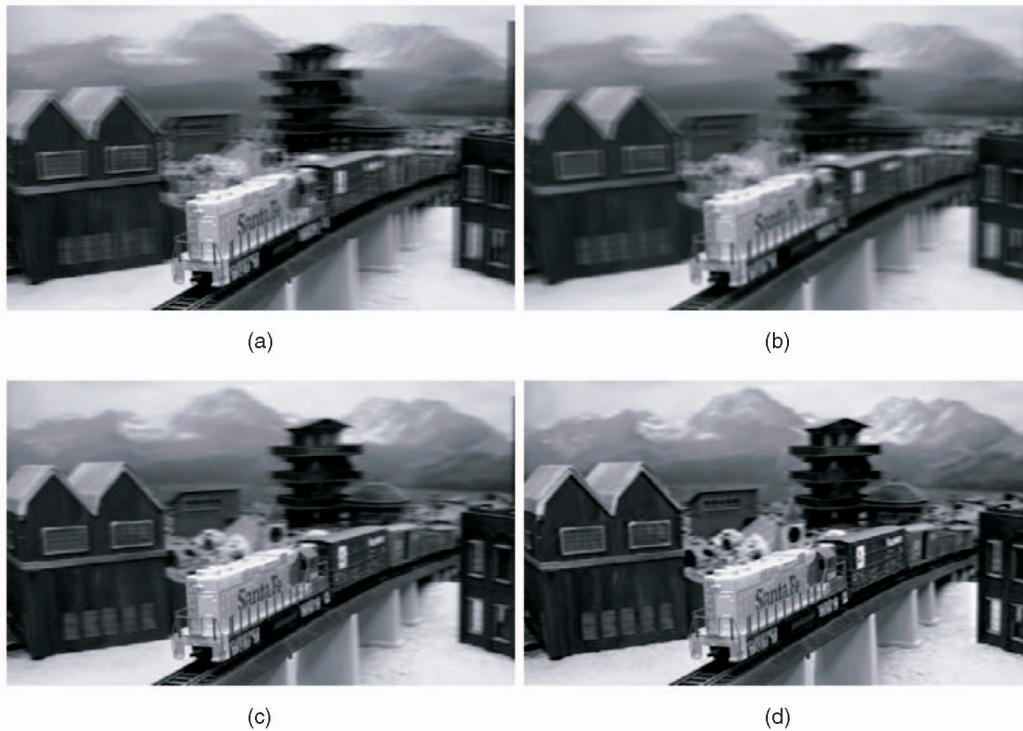


Fig. 10. Simulated multiview display of "Train" image. (a) The angular aliasing (double image) artifacts. (b) shows that light leakage decreases double images. (c) The antialiased light field (no double images, blurry due to angular PSF). (d) The proposed scheme (sharper output, angular PSF is precompensated). (a) Corrupted by aliasing (PSNR 25.22 dB). (b) Corrupted by aliasing and light leakage (PSNR 25.46 dB). (c) With antialias filter [5] (PSNR 25.81 dB). (d) With proposed prefilter after antialiasing (PSNR 26.35 dB).

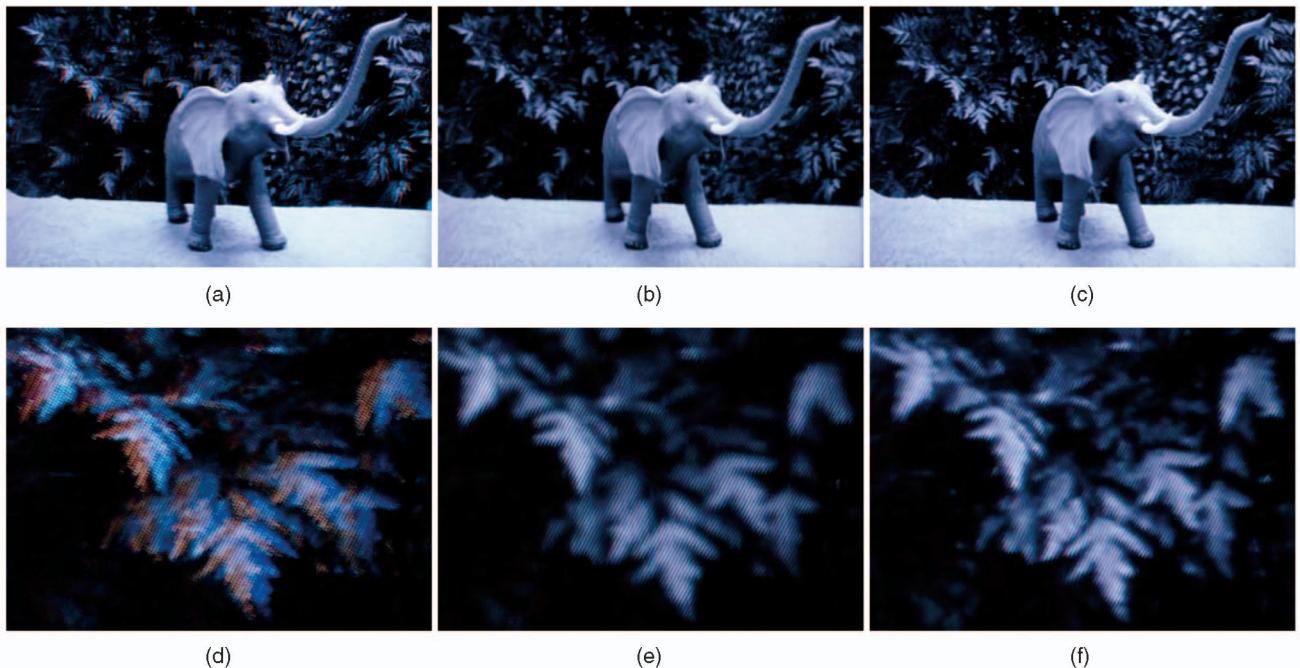


Fig. 11. High-resolution screen capture of "Elephant" image, shown in a Newsight parallax barrier multiview display. (a) and (d) The angular aliasing (double image) artifacts. (b) and (e) The antialiased light field (no double images, blurry due to angular PSF). (c) and (f) The proposed scheme (sharper output, angular PSF is precompensated). (a) No processing. (b) With antialias filter [5]. (c) With proposed prefilter. (d) No processing (zoomed). (e) With antialias filter [5] (zoomed). (f) With proposed prefilter (zoomed).

sharper at every depth. For example, the lettering that appear in the zoomed portions of Figs. 12d and 12e are illegible, but the prefiltering with (8) helps with the recovery of these letters.

Below is a brief summary of the real images captured on the 3D displays, in their order of appearance. Figs. 11 and 12 show the results captured on the parallax barrier display.

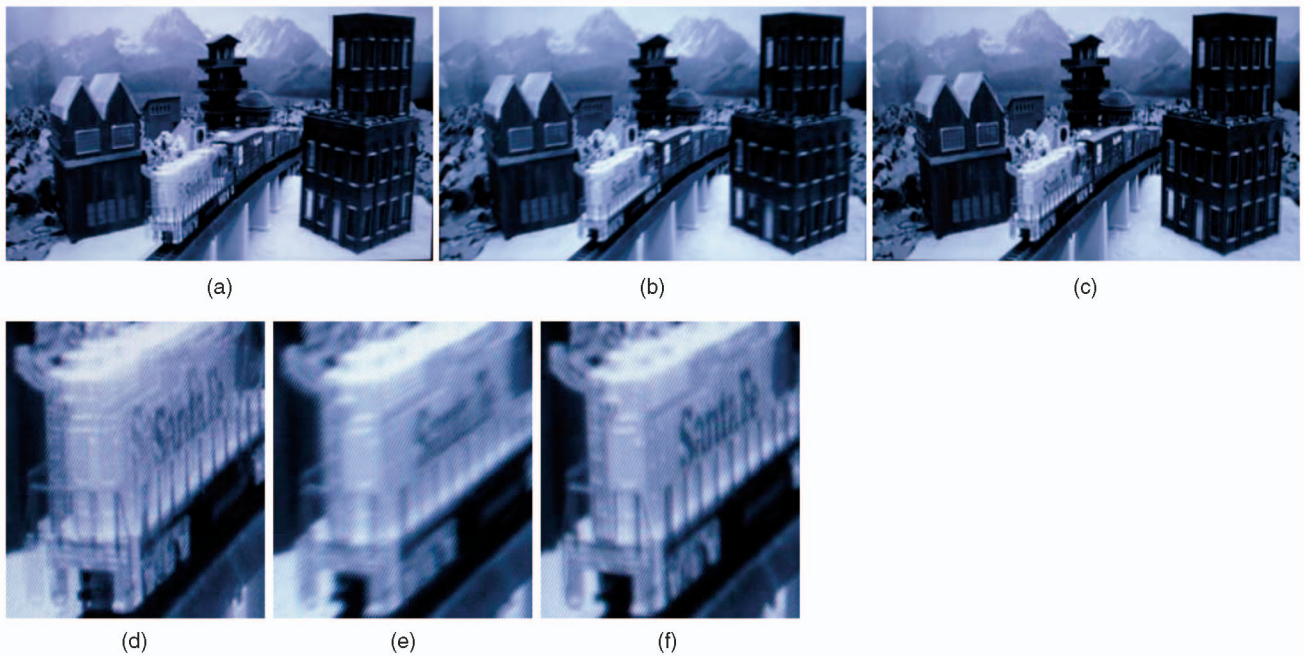


Fig. 12. High-resolution screen capture of “Train” image, shown in a Newsight parallax barrier multiview display. (a) and (d) The angular aliasing (double image) artifacts. (b) and (e) The antialiased light field (no double images, blurry due to angular PSF). (c) and (f) The proposed scheme (sharper output, angular PSF is precompensated). (a) No processing. (b) With antialias filter [5]. (c) With proposed prefilter. (d) No processing (zoomed). (e) With antialias filter [5] (zoomed). (f) With proposed prefilter (zoomed).

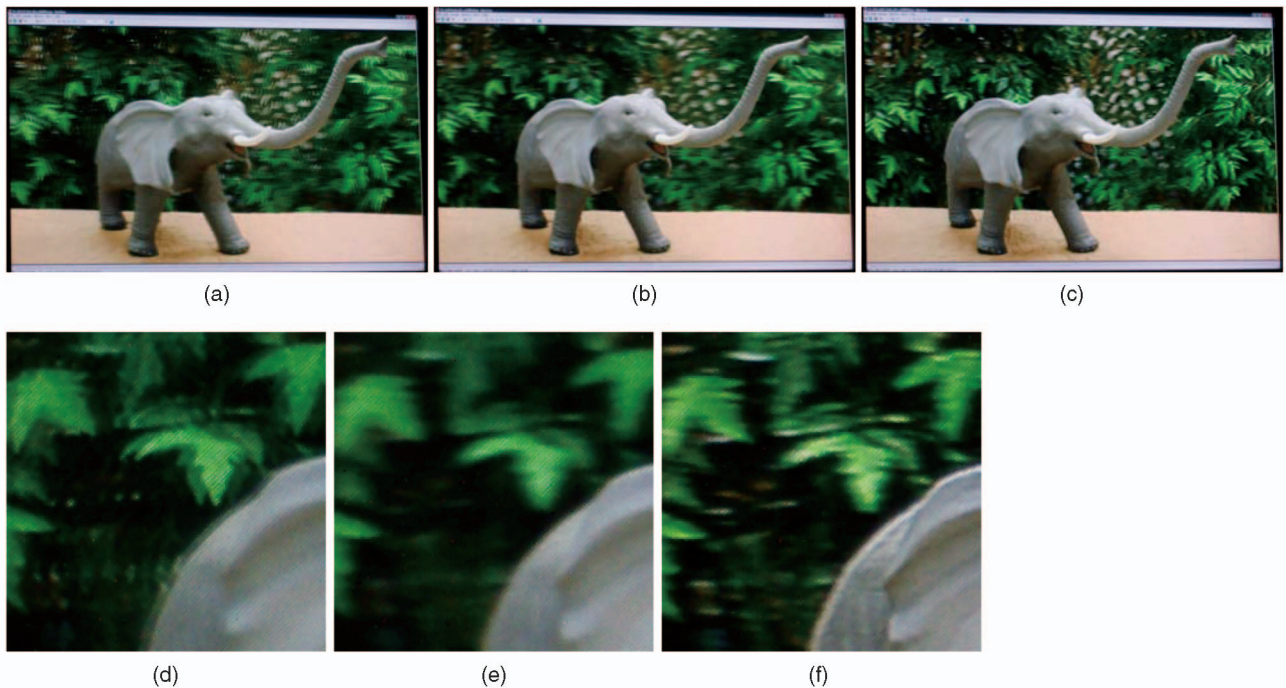


Fig. 13. High-resolution screen capture of “Elephant 2” image, shown in an Alioscopy lenticular multiview display. (a) and (d) The angular aliasing (double image) artifacts. (b) and (e) The antialiased light field (no double images, blurry due to angular PSF). (c) and (f) The proposed scheme (sharper output, angular PSF is precompensated). (a) No processing. (b) With antialias filter [5]. (c) With proposed prefilter. (d) No processing (zoomed). (e) With antialias filter [5] (zoomed). (f) With proposed prefilter (zoomed).

Figs. 11a, 11b, and 11c show the screen captures for the aliased light field, antialiased light field (affected by light leakage), and light field subject to the proposed angular sharpening prefilter as shown in the 3D display. Figs. 11c, 11d, and 11e show a certain portion of the captured images (aliased, antialiased, and prefiltered with the proposed

filter) for better comparison. All the above images are for the “Elephant” light field.

Figs. 12a, 12b, and 12c show the screen captures for the aliased light field, antialiased light field (affected by light leakage), and light field subject to the proposed angular sharpening prefilter as shown in the 3D display. Figs. 12c,

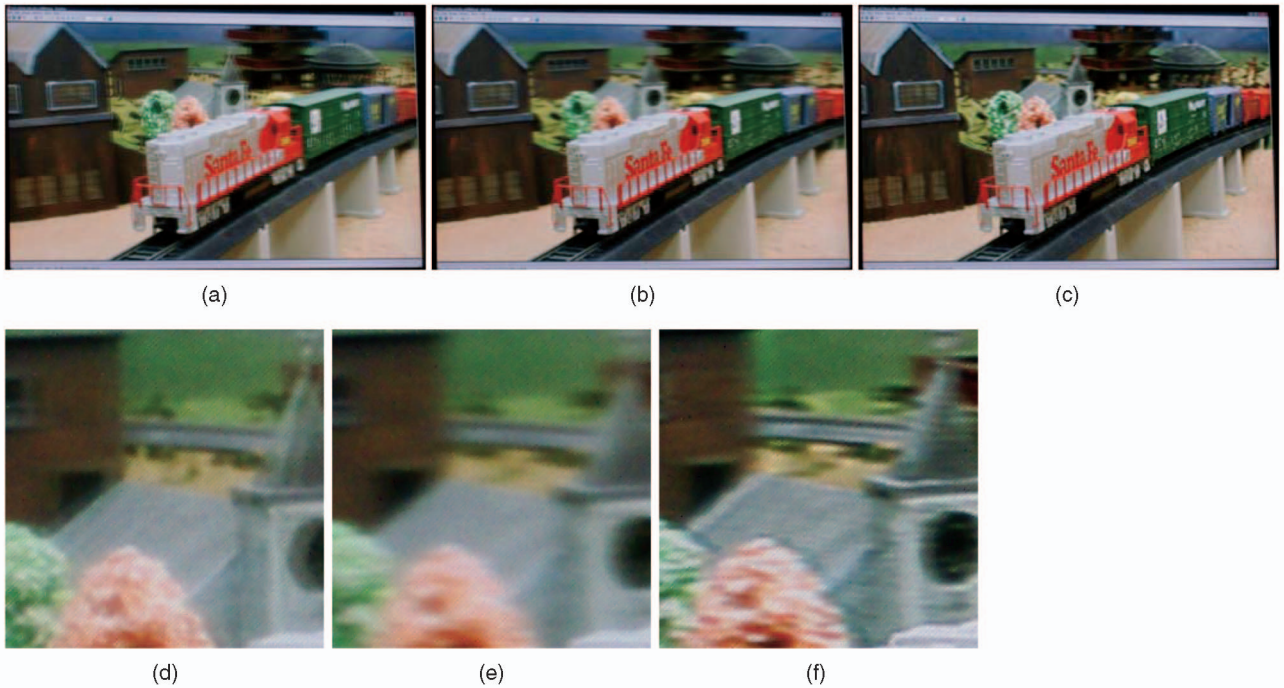


Fig. 14. High-resolution screen capture of "Train 2" image, shown in an Alioscopy lenticular multiview display. (a) and (d) The angular aliasing (double image) artifacts. (b) and (e) The antialiased light field (no double images, blurry due to angular PSF). (c) and (f) The proposed scheme (sharper output, angular PSF is precompensated). (a) No processing. (b) With antialias filter [5]. (c) With proposed prefilter. (d) No processing (zoomed). (e) With antialias filter [5] (zoomed). (f) With proposed prefilter (zoomed).

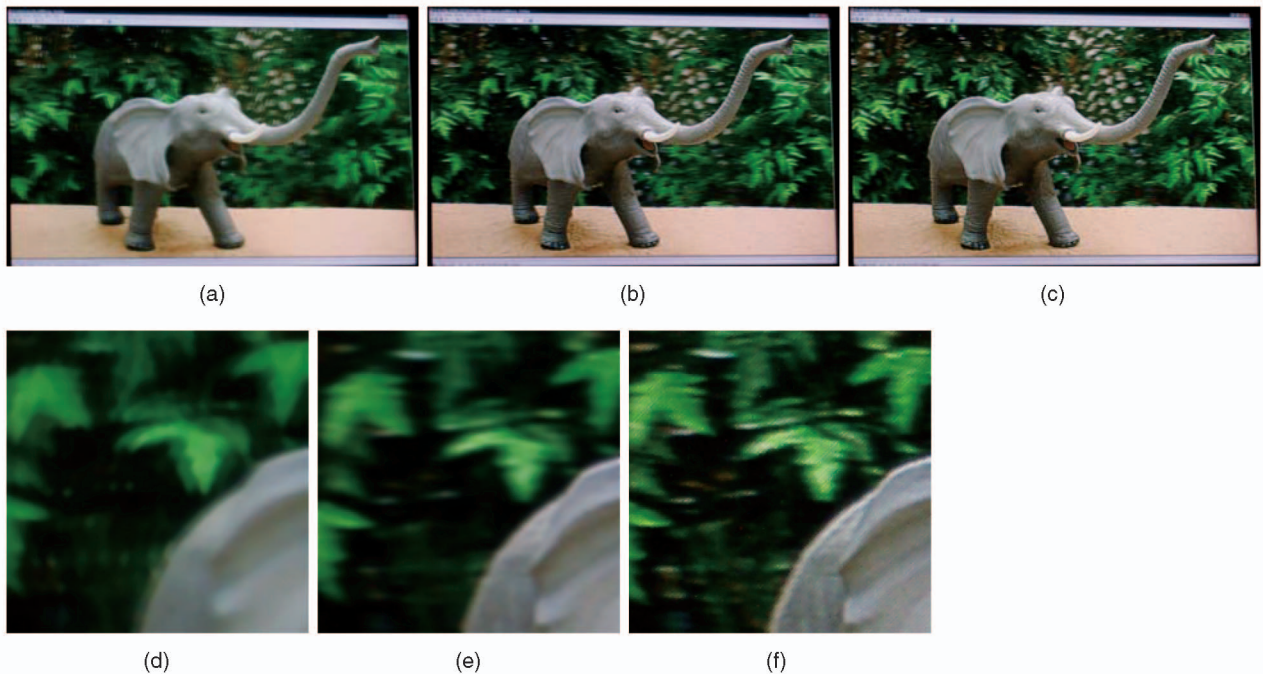


Fig. 15. Comparison of different filtering schemes for the "Elephant 2" image (Lenticular screen captures shown). (a) and (d) show the scheme by Boev et al. [1]. Notice the double images for regions away from the zero depth plane. (b) and (e) show the scheme by Jain and Konrad [4]. Regions away from the zero depth plane appear overly blurry. (c) and (f) show the proposed scheme, the image (for all regions of the 3D scene) is much sharper due to antialiasing and angular presharpener. (a) Method by Boev et al. [1]. (b) Prefilter by Jain and Konrad [4]. (c) Proposed prefilter. (d) Method by Boev et al. [1] (zoomed). (e) Prefilter by Jain and Konrad [4] (zoomed). (f) Proposed prefilter (zoomed).

12d, and 12e show a certain portion of the captured images (aliased, antialiased, and prefiltered with the proposed filter) for better comparison. All the above images are for the "Train" light field.

Figs. 13 and 14 show the results captured on the lenticular display.

Figs. 13a, 13b, and 13c show the screen captures for the aliased light field, antialiased light field (affected by light

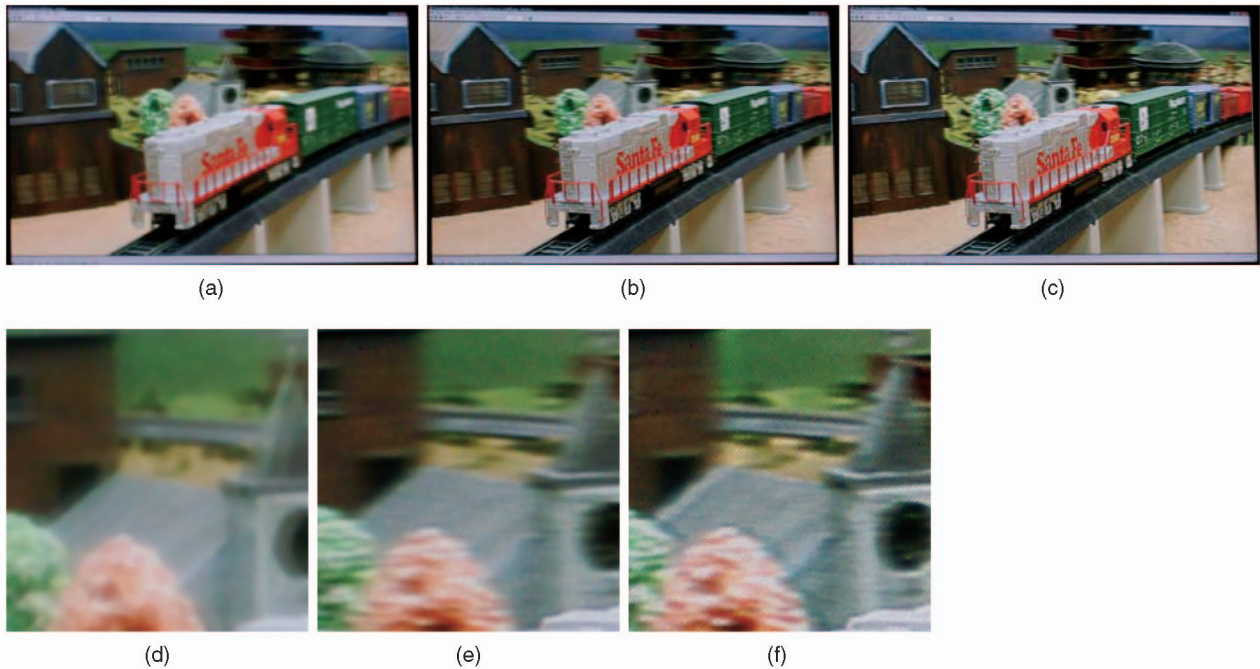


Fig. 16. Comparison of different filtering schemes for the “Train 2” image. Images shown are screen captures of the images displayed on an Alioscopy lenticular multiview display. (a) and (d) show the scheme by Boev et al. [1]. Notice the double images for regions away from the zero depth plane. (b) and (e) show the scheme by Jain and Konrad [4]. Regions away from the zero depth plane appear overly blurry. (c) and (f) show the proposed scheme, the image (for all regions of the 3D scene) is much sharper due to antialiasing and angular presharpening. (a) Method by Boev et al. [1]. (b) Prefilter by Jain and Konrad [4], (c) Proposed prefilter. (d) Method by Boev et al. [1] (zoomed). (e) Prefilter by Jain and Konrad [4] (zoomed). (f) Proposed prefilter (zoomed).

leakage), and light field subject to the proposed angular sharpening prefilter as shown in the 3D display. Figs. 13c, 13d, and 13e show a certain portion of the captured images (aliased, antialiased, and prefiltered with the proposed filter) for better comparison. All the above images are for the “Elephant 2” light field.

Figs. 14a, 14b, and 14c show the screen captures for the aliased light field, antialiased light field (affected by light leakage), and light field subject to the proposed angular sharpening prefilter as shown in the 3D display. Figs. 14c, 14d, and 14e show a certain portion of the captured images (aliased, antialiased, and prefiltered with the proposed filter) for better comparison. All the above images are for the “Train 2” light field.

Figs. 15 and 16 compare previous schemes in literature proposed by Jain and Konrad [4] (Figs. 15a and 16a) and Boev et al. [1] (Figs. 15b and 16b) with the proposed scheme (Figs. 15c and 16c) for the “Elephant 2” and “Train 2” light field, respectively. Figs. 15d, 15e, and 15f and 16d, 16e, and 16f show a zoomed in region for the three images processed using the schemes of Jain and Konrad, Boev et al., and the proposed scheme; for the “Elephant 2” and “Train 2” light fields, respectively. It is clear from the images that the proposed scheme offers a significant noticeable improvement over the other schemes in the literature.

## 5 CONCLUSION

In this work, a three-way interaction between the light field signal, the joint spatioangular sampling grid, and the interview light leakage in modern multiview 3D display

was characterized in the joint spatioangular frequency domain and with union of cosets. Stereoscopic image recovery is recast as a problem of joint spatioangular reconstruction, where the combination of the light leakage and human visual system provides the narrow-band filter. The nonidealities of this filter were corrected with the proposed prefiltering, which addresses aliasing and angular sharpening simultaneously. Finally, we confirmed the effectiveness of our approach in simulation and in physical hardware, and demonstrated improvement over existing techniques. Future work would involve a real-time GPU-based parallel implementation of the proposed algorithm, as well as extensions to volumetric displays which have both horizontal and vertical parallax.

## ACKNOWLEDGMENTS

Authors give sincere thanks to Dr. Janusz Konrad of Boston University for providing the help to understand [4] in depth.

## REFERENCES

- [1] A. Boev, K. Raunio, and K. Egiazarian, “GPU-Based Algorithms for Optimized Visualization and Crosstalk Mitigation on a Multiview Display,” *Proc. SPIE*, pp. 1-12, 2008.
- [2] J. Chai, X. Tong, S.C. Chan, and H. Shum, “Plenoptic Sampling,” *Proc. ACM SIGGRAPH '00*, pp. 307-318, 2000.
- [3] C. van Berkel and J.A. Clarke, “Characterization and Optimization of 3D-LCD Module Design,” *Proc. SPIE*, pp. 179-187, 1997.
- [4] A. Jain and J. Konrad, “Crosstalk in Automultiscopic 3D Displays: Blessing in Disguise?” *Proc. SPIE*, pp. 1-12, 2007.
- [5] M. Zwicker, W. Matusik, F. Durand, and H. Pfister, “Antialiasing for Automultiscopic 3D Displays,” *Proc. Eurographics Symp. Rendering*, 2006.

- [6] M. Halle, "Holographic Stereograms as Discrete Imaging Systems," *Proc. SPIE*, pp. 73-84, 1994.
- [7] C. Moller and A. Travis, "Correcting Interperspective Aliasing in Autostereoscopic Displays," *IEEE Trans. Visualization and Computer Graphics*, vol. 11, no. 2, pp. 228-236, Mar. 2005.
- [8] M. Zwicker, S. Yea, A. Vetro, C. Forlines, W. Matusik, and H. Pfister, "Display Pre-Filtering for Multi-View Video Compression," *Proc. 15th ACM Int'l Conf. Multimedia*, pp. 1046-1053, 2007.
- [9] M. Levoy and P. Hanrahan, "Light Field Rendering," *Proc. ACM SIGGRAPH '96*, pp. 31-42, 1996.
- [10] K. Hirakawa, "Crosstalk Explained," *Proc. IEEE Int'l Conf. Image Processing (ICIP '08)*, Oct. 2008.
- [11] J. Konrad and P. Agniel, "Subsampling Models and Anti-Alias Filters for 3D Automultiscopic Displays," *IEEE Trans. Image Processing*, vol. 15, no. 1, pp. 128-140, Jan. 2006.
- [12] E. Dubois, "The Sampling and Reconstruction of Time-Varying Imagery with Application in Video Systems," *Proc. IEEE*, vol. 73, no. 4, pp. 502-522, Apr. 1985.
- [13] R.L. De Valois and K.K. De Valois, *Spatial Vision*. Oxford Univ. Press, 1990.
- [14] O.H. Schade, "Optical and Photoelectric Analog of the Eye," *J. Optical Soc. of Am.*, vol. 46, pp. 721-739, Sept. 1956.



**Vikas Ramachandra** received the PhD degree from the UC San Diego in 2009. He presently works as a senior research engineer for the Multimedia R and D group at Qualcomm Inc. He has previously collaborated with researchers at HP Labs, MERL, and Nvidia Corp. His research interests include 3D image and processing for two-view and multiview displays and signal processing applications in computer vision.



**Keigo Hirakawa** received the BS degree in electrical engineering from Princeton University, the MM degree in jazz performance from the New England Conservatory of Music, and the PhD degree in electrical and computer engineering from Cornell University. He joined the University of Dayton as assistant professor of electrical and computer engineering in 2010. Prior to UD, he was with Harvard University as a research associate of Department of Statistics and School of Engineering and Applied Sciences. Previously, he was with HP/Agilent Technologies' camera division as an ASIC engineer. He has published in the fields of engineering, computer science, and statistics. He has received a number of recognitions, including a paper award from the IEEE and keynote speeches at IS&T CGIV, PCSJ-IMPS, and CSAJ sigFIV. He has strong track record of collaborating with industry partners. His research focuses on algorithmic development of image processing, computer vision, biomedical imaging, and sensor designs. He is best known for his expertise in digital camera designs, and his contributions span color science, estimation theory, statistical modeling, and wavelet theory. He is a member of the IEEE.



**Matthias Zwicker** received the graduate degree in computer science at ETH in Zurich, Switzerland, and the PhD degree from the same school. His PhD thesis focused on reconstruction, rendering, and editing of point-sampled geometry. From July 2003 to January 2006, he was a postdoctoral associate with the Computer Graphics Group at the Massachusetts Institute of Technology. Since September 2008, he is a professor at the University of Bern in Switzerland. He is an adjunct faculty with the Computer Graphics Laboratory at the University of California in San Diego. He is a member of the IEEE.



**Truong Nguyen** received the PhD degree from Caltech in 1989. He came to the Jacobs School at the UC San Diego in 2001. He manages the Video Processing Group, and teaches courses associated with the Signal Image Processing Program (SIP). He is a 1995 recipient of the US National Science Foundation (NSF) career award and is coauthor of a popular book: *Wavelets and Filter Banks*, and author of several matlab-based toolboxes on image compression, electrocardiogram compression, and filter bank design. He also holds a patent on an efficient design method for wavelets and filter banks and several patents on wavelet applications including compression and signal analysis. He is a fellow of the IEEE.

► **For more information on this or any other computing topic, please visit our Digital Library at [www.computer.org/publications/dlib](http://www.computer.org/publications/dlib).**